ACS APPLIED MATERIALS & INTERFACES

www.acsami.org

Research Article

Tuning the Crystallinity and Coverage of SiO_2–$ZnIn_2S_4$ Core–Shell Nanoparticles for Efficient Hydrogen Generation

Mrinalini Mishra,[‖] Yen-Chen Huang,[‖] Peng-Hua Wang, Si-Ping Liu, T. Randall Lee, and Tai-Chou Lee*

Cite This: *ACS Appl. Mater. Interfaces* 2021, 13, 4043–4050

Read Online

ACCESS | Metrics & More | Article Recommendations | Supporting Information

ABSTRACT: The coverage, thickness, and crystallinity of $ZnIn_2S_4$ (ZIS) shells on SiO_2 core nanoparticles (SiO_2@ZIS) were systematically investigated using microwave-assisted solvothermal methods aided by the addition of acid in ethanolic medium. The surface modification of the SiO_2 cores with (3-mercaptopropyl)-trimethoxysilane was found to be critical to generate a homogeneous coverage of $ZnIn_2S_4$. The SiO_2@ZIS core–shell nanoparticles exhibited the best coverage but poor crystallinity when synthesized in pure ethanol, whereas best crystallinity but poor coverage was observed when synthesized in an aqueous solution. The addition of selected amounts of acid (HCl) led to improved crystallinity in the ethanolic medium. The thickness of the ZIS shell could be controlled in an ethanolic solution by judiciously varying the amounts of acid and the concentration of the ZIS precursor. Increasing the concentration of the ZIS precursor to twice the standard concentration in ethanolic solution with the addition of 100 μL of HCl afforded better crystallinity, homogeneous coverage, and optimal photocatalytic hydrogen production.

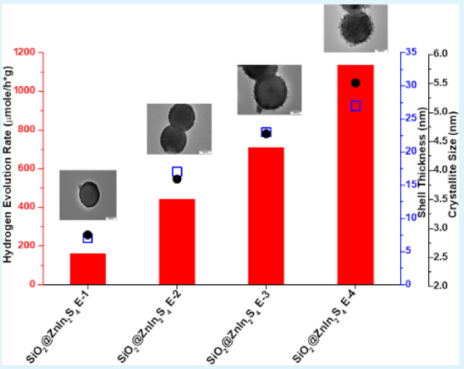

KEYWORDS: *core–shell nanoparticles, $ZnIn_2S_4$ shells, silica cores, photocatalytic hydrogen evolution*

INTRODUCTION

In the 21st century, new environmental issues are emerging, and climate change concerns are becoming more and more important. Of the current alternative energy sources, hydrogen is the most important, as it is a clean energy source obtained by the conversion of sustainable solar energy.[1−3] In contrast to metal oxides that are mostly UV-active, metal sulfides are attractive photocatalysts because they possess suitable energy gaps for visible-light response.[4−7] Especially, ternary sulfide $ZnIn_2S_4$ (ZIS) is considered as an efficient visible-light-driven photocatalyst.[8−10] In efforts to boost hydrogen evolution, $ZnIn_2S_4$ has been doped,[9,11,12] prepared as various heterostructures[13−16] and core–shell structures,[17,18] synthesized using surfactants,[19−21] and modified with noble metal cocatalysts.[17,22]

Unfortunately, most photocatalysts suffer from fast recombination kinetics, which decreases hydrogen production.[3,4,17,22,23] However, unique core–shell structures with surface plasmon resonance (SPR) properties can mitigate the problem.[17] SPR excited by incident light can generate strong electric fields close to the metal surface, along with the resonance energy transfer, which can facilitate charge separation and improve light absorption.[24−26] In our previous work,[17] we developed a method to synthesize core–shell nanoparticles having noble metal cores and ZIS shells. Gold–silver nanoshells (GS-NS) with SPR and tunable absorption embedded in a ZIS matrix demonstrated that the coupling between the SPR of the GS-NS and the absorption of the ZIS photocatalyst was the key parameter to optimize solar hydrogen production. However, the coverage and thickness of the ZIS shells on GS-NS cores were not precisely controlled. In this work, we focused on preparing SiO_2 core–ZIS shell nanoparticles with ZIS shells having tunable thickness as this limits the range of electric field around the metal surface. In addition to the tunable ZIS shell thickness, we also focused on better coverage and crystallinity of SiO_2@ZIS to enhance the SPR effect and consequently hydrogen production.

First, we sought to optimize the deposition of ZIS shell on SiO_2 cores by examining various solvent media. Literature studies focusing on the synthesis of ZIS in various solutions have explored the use of, for example, water, methanol, and ethanol.[27] The studies found that ZIS synthesized in water has better crystallinity and hydrogen production than ZIS synthesized in organic solvents, but there was no mention of the coverage of ZIS when coated onto other materials. Our preliminary data showed that coating ZIS onto SiO_2 cores in ethanol offered good coverage compared to water but poor

Received: November 20, 2020
Accepted: December 31, 2020
Published: January 15, 2021

https://dx.doi.org/10.1021/acsami.0c20716
ACS Appl. Mater. Interfaces 2021, 13, 4043–4050

crystallinity and limited hydrogen production. In water, ZIS synthesized under acidic conditions exhibited enhanced crystallinity and hydrogen production.[28−30] In the present study, we explored the addition of HCl to ethanol for improving the crystallinity of ZIS while maintaining good coverage. We found that adding suitable amounts of HCl in ethanol solution is an innovative method to synthesize ZIS with enhanced crystallinity and good coverage on SiO_2 cores; importantly, the resultant core−shell nanoparticles exhibited enhanced photocatalytic hydrogen production.

EXPERIMENTAL SECTION

Preparation of Modified Silica Core Nanoparticles. The preparation of silica nanoparticles followed the Stöber method[31] and the work of Kim et al.[32] Typically, 200 mL of ethanol and 18 mL of ammonium hydroxide were mixed in a round-bottom flask by stirring for 5 min. Then, 6.8 mL of tetraethoxysilane ($Si(OC_2H_5)_4$) was added and maintained at 30 °C. This mixture was stirred overnight. To further modify SiO_2, 250 μL of (3-mercaptopropyl)trimethoxysilane ($C_6H_{16}SO_3Si$, MPS) was added into the mixture while stirring for 6 h at 30 °C. The temperature was then raised to 88 °C for 1 h under reflux to strengthen the covalent bonding. The cooled-down mixture was then centrifuged at 2500 rpm for 1 h to remove excess MPS. The precipitate was collected and re-dispersed into 50 mL of ethanol to obtain an MPS-modified SiO_2 suspension. To ascertain the amount of SiO_2 in ethanol, 5 mL of SiO_2 ethanol suspension was dried in an oven and weighed. The gross amount of SiO_2 was calculated, and an appropriate amount of ethanol was further added to confirm that there was 0.1 g SiO_2 in 5 mL of the SiO_2−ethanol suspension.

Preparation of SiO_2@ZIS Core−Shell Nanoparticles. In preparing bare ZIS particles, zinc nitrate hexahydrate (0.3 mmol), indium (III) nitrate hydrate (0.6 mmol), and thioacetamide (TAA, 2.4 mmol) were dissolved in 15 mL of water or ethanol under vigorous stirring for 10 min. This concentration of precursors is denoted as the standard concentration for our experiments. Note that water and ethanol are the preferred solvents in the work owing to their low toxicity and price. Further, water has a high dielectric constant and hence offers good dissolution of the precursors. However, ethanol has a relatively lower dielectric constant, but owing to its low boiling point, the solubility of precursors increases as the internal pressure increases at a fixed temperature during the solvothermal reaction. Furthermore, ethanol has a high dielectric loss tangent that allows it to utilize microwave well. The solution was then poured into a 30 mL quartz vessel. The hydrothermal reaction was carried out in a microwave reactor (Monowave 300, Anton Paar) at 120 °C for 10 min. The precipitates were collected and centrifuged at 8000 rpm for 10 min. The obtained particles were rinsed thoroughly with deionized (DI) water several times and were then dried in an oven at 80 °C for 12 h. For the synthesis of SiO_2@ZIS nanoparticles, 5 mL of SiO_2 ethanol suspension (0.1 g SiO_2 nanoparticles) were re-dispersed in 10 mL of ethanol solution using ultrasonic vibration. For synthesis in water, 0.1 g SiO_2 (obtained by drying 5 mL of SiO_2 ethanol suspension) was dispersed in 15 mL of water. Then, zinc, indium, and sulfur precursors were added following the same procedure as in the case of preparing bare ZIS particles along with a certain amount of HCl. The parameters for microwave-assisted hydrothermal reaction, collection, and drying were also the same as those for synthesizing bare ZIS particles. A simple nomenclature was followed for labeling all samples. Samples synthesized with 15 mL of water and ethanol were denoted by "W" and "E", respectively. The addition of selected amounts, 0, 20, 50, and100 μL, of HCl was indicated by 1, 2, 3, and 4, respectively. For example, SiO_2@ZIS E-3 sample is ZIS coated on SiO_2 in 15 mL of ethanol solution in which 50 μL of HCl was added.

Further, in an effort to control and study the effects of the ZIS shell thickness, we increased the concentration of the precursor for ZIS by 2 and 3 times the standard concentration for varying amounts of HCl addition, and the sample names were annotated with 2×ZIS and 3×ZIS, respectively.

Characterizations. Extinction spectra were obtained using a UV−visible spectrophotometer (Jasco V-670) over the wavelength range of 400−700 nm. Nanoparticles were dispersed in DI water or ethanol, and particle size was measured using dynamic light scattering (Malvern Nano-ZS9). Crystal structures were analyzed using an X-ray diffractometer (Bruker KAAPA APEX II). A Cu Kα X-ray source coupled with a Ni filter was used. The scan rate was set at 3 °C/min in the 2θ range of 10°−80°. A transmission electron microscope (JEOL-JEM2000) and a high-resolution transmission electron microscope (JEOL-JEM2100) operated at an accelerating voltage of 200 kV were used to observe the morphology of the nanoparticles. Energy-dispersive X-ray spectroscopy (EDS) was performed on the high-resolution transmission electron microscope as well. An X-ray photoelectron spectroscope (Thermo VG-Scientific/Sigma Probe) with an Al Kα (1486.6 eV) X-ray source was used to determine the surface composition of bare SiO_2 and MPS-modified SiO_2. A Fourier transform infrared (FTIR) spectroscope (Perkin-Elmer Instruments LLC, Shelton, CT) was used to observe the complex formation of TAA with metal ions. For this, the ZIS precursor in water or ethanol along with SiO_2 nanoparticles was detected by FTIR spectroscopy.

Photocatalytic Hydrogen Generation. The photocatalytic reaction of hydrogen production was conducted in a 300 mL custom-built two-neck cylindrical glass cell with a quartz side window and an illumination area of 27.7 cm^2. The sacrificial agent was prepared by adding potassium sulfite (0.25 M) and sodium sulfide (0.35 M) in DI water (220 mL). A 0.03 g of prepared ZIS or SiO_2@ZIS particles was dispersed in the sacrificial solution, and an appropriate amount of dihydrogen hexachloroplatinate(IV) hexahydrate was added. The reactor was then connected to cold traps to prevent vapors from coming into the gas chromatography (GC) column. The whole system was operated in a low-pressure condition with a gas circulation pump. The photocatalytic reactor was irradiated by a 300 W Xe lamp. The intensity was set at 100 mW/cm^2 and measured by an optical meter (Newport 1918-R). The temperature was kept at 25 °C during the reaction, and hydrogen gas was collected using an online GC system (China 8700F GC). Figure S1 shows the schematic of the hydrogen generation setup.

RESULTS AND DISCUSSION

The silica core nanoparticles were prepared using the modified Stöber method, as described in the Experimental Section. The products were analyzed by TEM to determine whether the size and morphology were similar to the GS-NSs. As illustrated in Figure S2, the average particle size for the silica nanoparticles was 177 ± 26 nm, and the associated particle size distribution histograms are provided in Figure S3 and Table S1 in the Supporting Information. In this work, we coated ZIS on silica cores as a model system for ZIS coated on the surface of GS-NS@SiO_2 nanoparticles. Hence, an important comparison with our previous work showed that the diameter of the SiO_2 cores is nearly the same as that of the GS-NS@SiO_2 cores when the SiO_2 shell thickness was 47 nm.[17] The surface of the SiO_2 cores was modified using MPS to generate core SiO_2 exposing multiple thiol groups.[33−37] The morphology of silica cores without and with modification is shown in Figure S4a,b, where no obvious differences are discernible. In contrast, Figure S5 shows the XPS spectra of the two samples. For silica with modification, a weak S 2p peak at the binding energy = 162−163 eV appeared, which can be attributed to the −SH functional group of MPS on the SiO_2 cores.

SiO_2@ZIS Core−Shell Nanoparticles. In our previous study,[17] we have successfully prepared ZIS shells on GS-NS cores in water using the standard ZIS precursor concentration, as described in the Experimental Section. However, the uniform coverage and thickness of ZIS were not yet optimized.

https://dx.doi.org/10.1021/acsami.0c20716
ACS Appl. Mater. Interfaces 2021, 13, 4043−4050

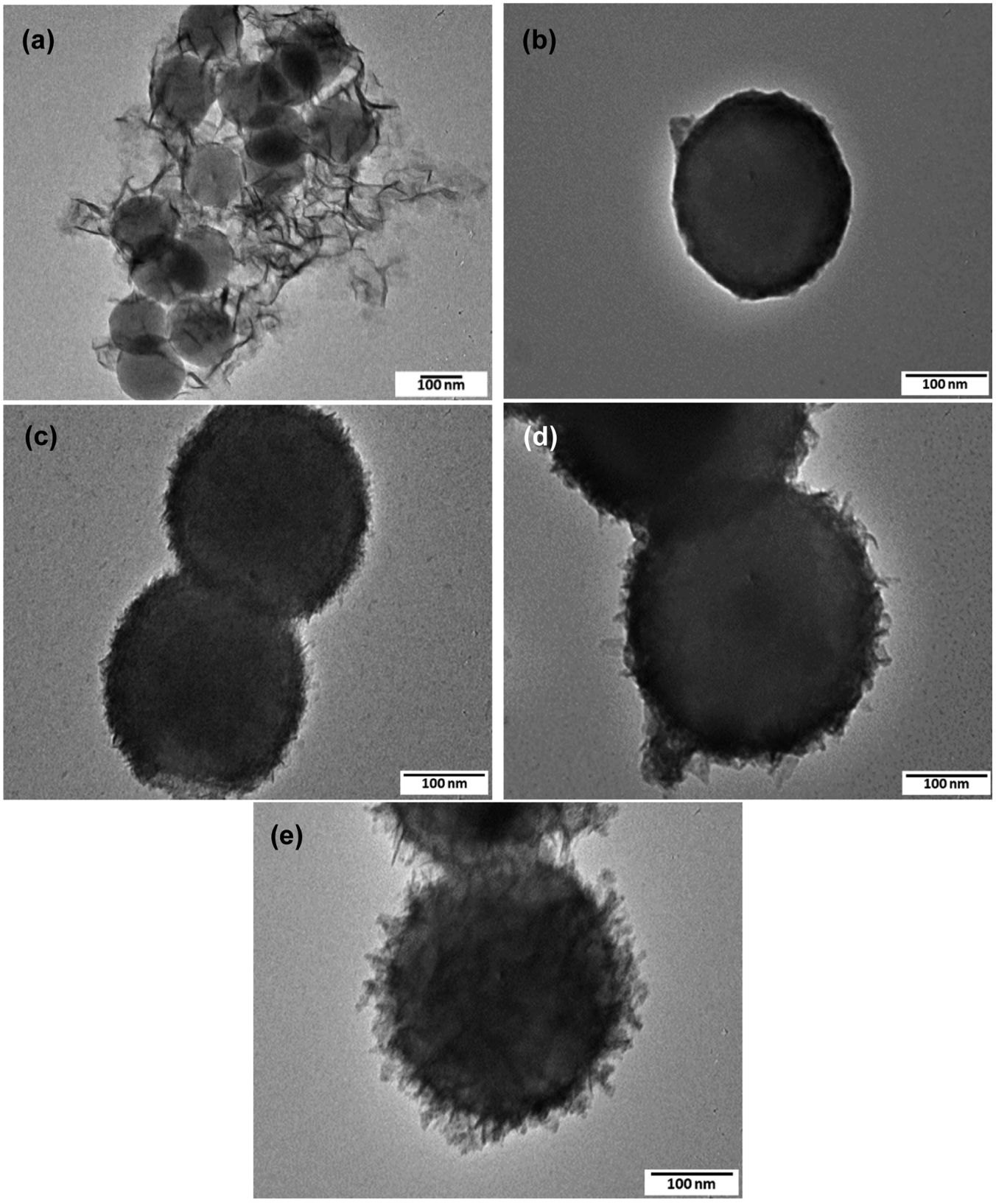

Figure 1. TEM images of (a) SiO_2@ZIS W-1, (b) SiO_2@ZIS E-1, (c) SiO_2@ZIS E-2, (d) SiO_2@ZIS E-3, and (e) SiO_2@ZIS E-4 nanoparticles.

To clearly demonstrate the critical role of MPS modification on the SiO_2 surface, a lower ZIS precursor concentration was used. Here, 1/10 of the standard concentration was utilized to coat ZIS on bare and MPS-modified SiO_2 core particles in water. Figure S6a shows that SiO_2 particles without modification lead to the aggregation of ZIS and a rough morphology. However, SiO_2 particles with surface modification show homogeneous coverages, as illustrated in Figure S6b. Hence, it could be presumed that the precursor of ZIS preferably adsorbs on the thiol groups, circumventing the

https://dx.doi.org/10.1021/acsami.0c20716
ACS Appl. Mater. Interfaces 2021, 13, 4043−4050

random growth of ZIS on SiO_2. However, Figure 1a shows that upon increasing the ZIS precursor to a standard concentration in aqueous solution, ZIS failed to grow uniformly on the SiO_2 cores. For a core−shell composite photocatalyst, it is important to control the coverage, as it influences the catalytic efficiency.[18,38] Further, crystallinity is also critical to enhance hydrogen production.[27,39] Hence, we used ethanol and HCl in an effort to enhance the coverage and crystallinity of core−shell SiO_2@ZIS composites as compared to those synthesized in water.[28−30]

Now, we compare the core−shell structures of SiO_2@ZIS synthesized in water (W) and ethanol (E). The coverage and crystallinity of ZIS in SiO_2@ZIS W-1 and SiO_2@ZIS E-1 were characterized by TEM (Figure 1a,b) and XRD (Figure 2). The

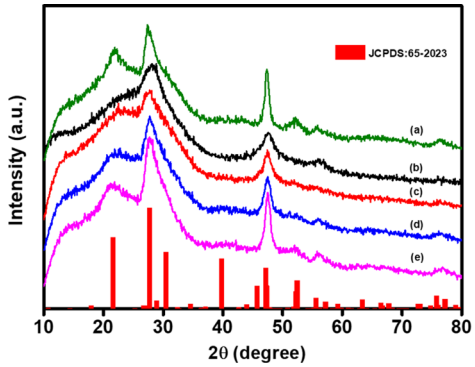

Figure 2. XRD patterns of (a) SiO_2@ZIS W-1, (b) SiO_2@ZIS E-1, (c) SiO_2@ZIS E-2, (d) SiO_2@ZIS E-3, and (e) SiO_2@ZIS E-4.

XRD patterns were indexed to hexagonal $ZnIn_2S_4$ (JCPDS no. 65-2023). Figures 1a,b and 2 show that SiO_2@ZIS synthesized in water has better crystallinity but worse coverage compared to SiO_2@ZIS synthesized in ethanol. Although SiO_2@ZIS synthesized in ethanol has good coverage, poor crystallinity would limit hydrogen production.[27,39] Thus, we added HCl to the ethanolic reaction medium in an effort to enhance the crystallinity as in the case of water.[28−30]

A progressive enhancement of coverage with respect to HCl addition is evident from Figure 1b−e, which shows the TEM images of SiO_2@ZIS (E-1 to E-4). We also used TEM imaging to determine the thickness of the ZIS shell on SiO_2 by calculating the difference in the diameters of SiO_2@ZIS and bare SiO_2. It was found that larger amounts of HCl in ethanol led to thicker ZIS shells. Figure 2 shows that the crystallinity increased with increasing amounts of HCl added. Sample SiO_2@ZIS E-4 has crystallinity similar to the samples synthesized in an aqueous solution. Table 1 provides the

Table 1. The d(102) Crystallite Size of SiO_2@ZIS Nanoparticles Synthesized under Various Conditions

SiO_2@ZIS	W-1	E-1	E-2	E-3	E-4
mean crystallite size, d(102) (nm)	5.05	2.89	3.85	4.63	5.51

d(102) crystallite sizes calculated according to the Scherrer equation. Sample SiO_2@ZIS E-4 has the largest crystallite size. Figure 3a−d shows the HRTEM images and the EDS line scans of SiO_2@ZIS synthesized in ethanol by adding 100 μL of HCl (SiO_2@ZIS E-4). The HRTEM images confirm that the shell growing on SiO_2 is indeed ZIS. Thus, SiO_2@ZIS nanoparticles synthesized in ethanol with increasing amounts of HCl have better ZIS coverage along with better ZIS crystallinity when grown on MPS-modified SiO_2 cores. The increasing amount of HCl added to the ethanol medium improved the crystallinity as TAA (CH_3CSNH_2) contributes to the release of H_2S gas during hydrothermal processes in the presence of larger amounts of acid.[40,41] The concentration of hydrochloric acid used here is ∼35%. There is still some water present that can initiate the reaction with TAA to produce H_2S gas. Sufficient gas leads to higher pressure inside the reaction vessel, which in turn leads to ZIS with better crystallinity and tendency to grow on the SiO_2 cores.[28] Note that upon further addition of HCl above 100 μL, the uniformity of ZIS deposition on the SiO_2 surface was lost. Figure S7 shows the TEM image of SiO_2@ZIS synthesized in ethanol with 150 μL of HCl. We speculate that adding 150 μL of HCl hastens the production of H_2S.

To further investigate the enhanced coverage of ZIS on MPS-modified SiO_2 when synthesized in ethanol, the precursor mixtures in water and ethanol were analyzed separately by FTIR analysis (Figure 4). Figure 4 shows two additional peaks at 1320 and 1645 cm^{-1} in ethanol. It has been reported that zinc forms a complex with TAA, and its corresponding FTIR peak appears at 1645 cm^{-1}.[42] Further, Chen et al. evaluated the time-dependent evolution of chemical species through SEM and EDS during the synthesis of ZIS.[30] Based on their observations, they proposed that zinc and indium form three different complexes with TAA: tetrahedral $[Zn(TAA)_4]^{2+}$, tetrahedral $[In(TAA)_4]^{3+}$, and octahedral $[In(TAA)_6]^{3+}$. Hence, we hypothesize that the peak at 1320 cm^{-1} is from the complex formed between indium and TAA; however, we can find no literature to support this hypothesis. Thus, zinc and indium ions form complexes with TAA in ethanolic solution before and/or during the hydrothermal process, leading to a slower and a more homogeneous coating. It is plausible that the complexes of zinc and indium with TAA attach to the surface of MPS-modified SiO_2 owing to the surface modification. During the hydrothermal process, the small amounts of water present in HCl added to ethanol initiate the hydrolysis of TAA more slowly than that in water alone, which leads to a slow reaction between the metal ion and H_2S. Consequently, SiO_2@ZIS has a better ZIS coverage in ethanol than in water.

The energy band gap is also an important factor for photocatalytic hydrogen production.[4,23] The Kubelka−Munk plot in Figure 5 reveals that the energy band gap of SiO_2@ZIS synthesized in HCl-treated ethanolic solution is ∼2.2−2.4 eV, which is comparable to that of SiO_2@ZIS synthesized in aqueous solution (2.25 eV).[17] Notably, all are in the range of visible light. Furthermore, to study the effect of ZIS shell thickness, the concentration of ZIS precursor was also varied for SiO_2@ZIS synthesized in ethanolic solution with 100 μL of HCl. Figure 6a−c shows the TEM images of samples prepared with higher concentrations of ZIS precursor. The ZIS shell got thicker with the increasing concentration of ZIS precursor (see Table S2). Nonetheless, the increasing shell thickness had no effect on crystallinity (see Figure 6d) and the energy band gap (see Figure 6e).

Photocatalytic Hydrogen Evolution. Figure 7 shows the photocatalytic hydrogen evolution rate of SiO_2@ZIS synthesized in ethanol with varying amounts of HCl. SiO_2@ZIS nanoparticles synthesized in ethanolic solution with no or small amounts of HCl have low hydrogen evolution rates, whereas the addition of larger amounts of HCl improves the

https://dx.doi.org/10.1021/acsami.0c20716
ACS Appl. Mater. Interfaces 2021, 13, 4043−4050

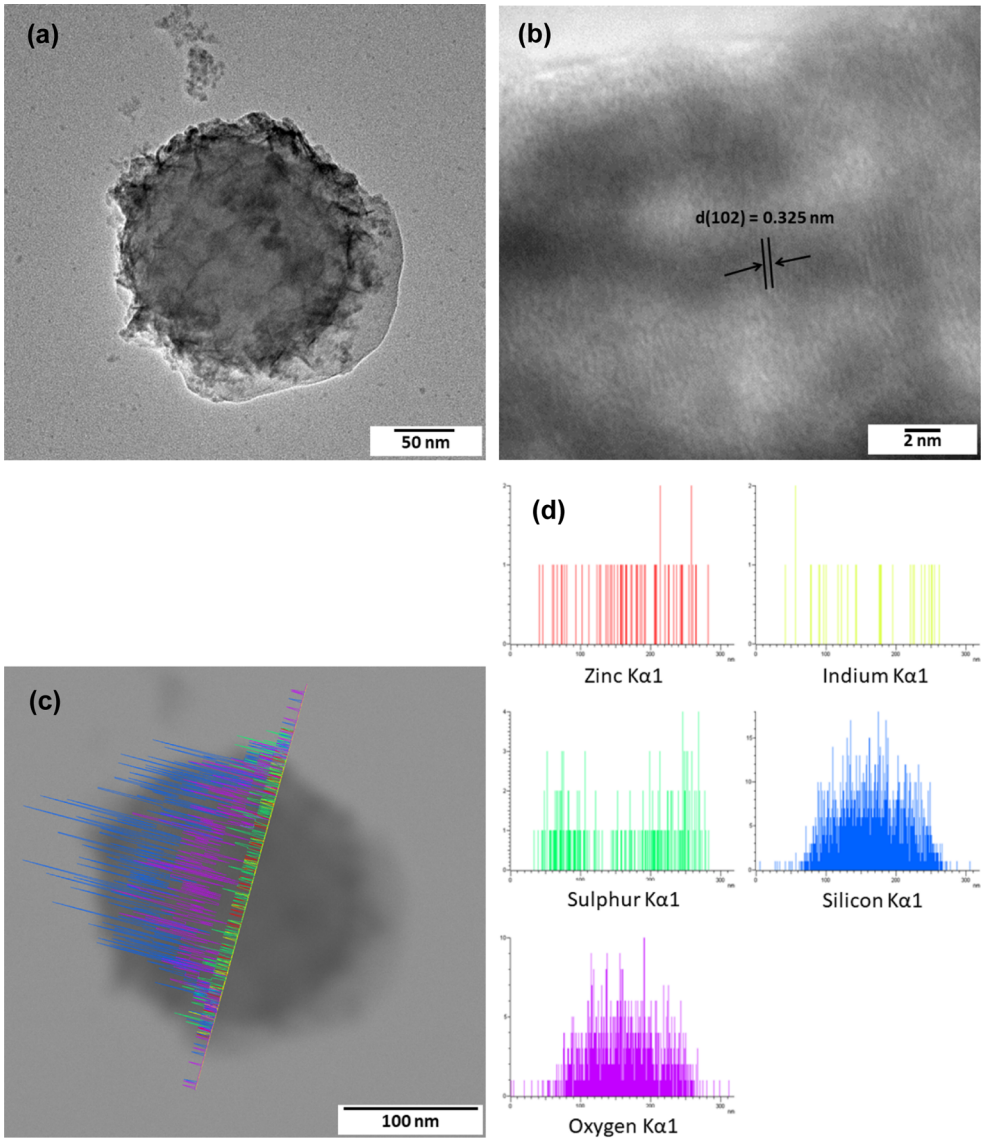

Figure 3. (a) TEM image, (b) HRTEM image, (c) representative line scan TEM image, and (d) EDS line scan of SiO_2@ZIS E-4 nanoparticles.

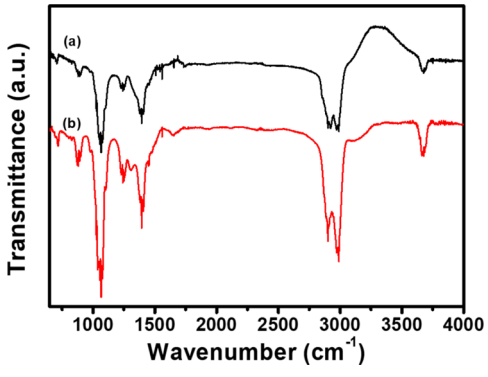

Figure 4. FTIR spectra of MPS-modified SiO_2 with ZIS precursor in (a) water and (b) ethanol.

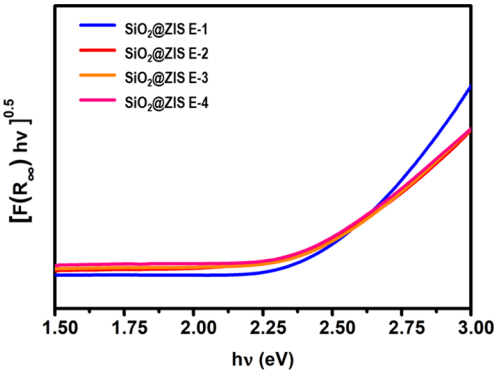

Figure 5. UV−Vis spectra for SiO_2@ZIS nanoparticles synthesized in ethanol with varying amounts of HCl.

hydrogen evolution rate, with the sample SiO_2@ZIS E-4 exhibiting the highest hydrogen evolution rate of all. The shell thickness of ZIS for the samples synthesized in ethanolic solution is also shown in Figure 7. As noted above, we expect the crystallinity of ZIS to be a critical factor affecting the hydrogen evolution rate of SiO_2@ZIS. Accordingly, sample SiO_2@ZIS E-4 exhibited ~3.1 times higher hydrogen evolution rate compared to bare ZIS. A correlation between the XRD pattern (Figure 2) and the hydrogen evolution rates (Figure 7) shows that better crystallinity leads to greater hydrogen

https://dx.doi.org/10.1021/acsami.0c20716
ACS Appl. Mater. Interfaces 2021, 13, 4043−4050

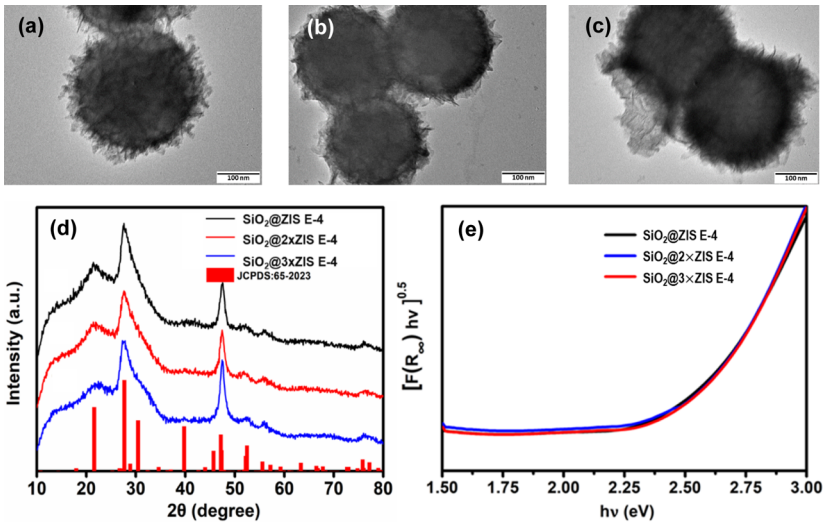

Figure 6. SiO_2@ZIS core−shell nanoparticles synthesized using varying concentrations of precursors in ethanol with 100 μL HCl: TEM images (a) SiO_2@ZIS E-4 (b) SiO_2@2xZIS E-4, and (c) SiO_2@3xZIS E-4. (d) XRD patterns and (e) UV−Vis spectra.

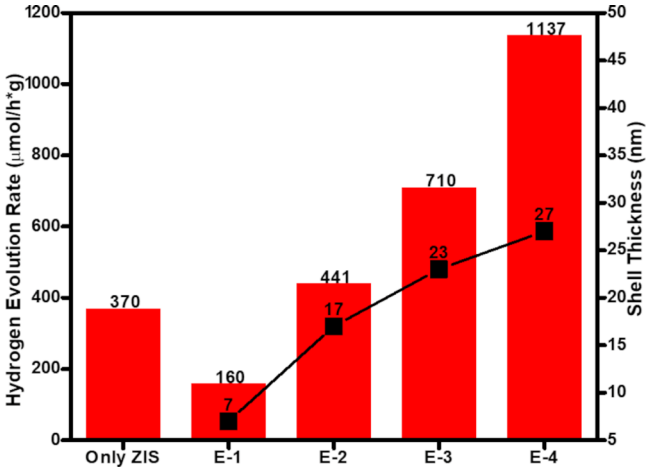

Figure 7. Photocatalytic hydrogen evolution rate (calculated based on the amount of ZIS in the composite) of SiO_2@ZIS in ethanol with different amounts of HCl. The ZIS shell thicknesses are also indicated.

evolution. Furthermore, we can infer from Figure 4 that SiO_2@ZIS nanoparticles synthesized in ethanol with larger amounts of HCl bearing thicker ZIS shells give the greatest overall rate of hydrogen evolution. As such, we chose to examine the effect of ZIS shell thickness on hydrogen evolution in detail.

The ZIS shell thickness, morphology, and hydrogen evolution rates for the samples synthesized with varying amounts of HCl and varied concentrations of ZIS precursor are shown in Table S2 and Figures S8 and S9. The normalized hydrogen evolution rates of the samples synthesized with 100 μL of HCl for various concentrations of ZIS precursors are also shown in Table S2. The sample SiO_2@ZIS E-4 exhibited the greatest hydrogen evolution rate when synthesized at 2 times the initial concentration of ZIS precursor. However, there seems to be a critical shell thickness that is beneficial to hydrogen evolution. The hydrogen generation rate decreased upon further increasing the concentration of ZIS precursor and thereby the ZIS shell thickness. Further, a careful observation of Figure S8 reveals that the ZIS shell appears to be more loosely packed when synthesized with larger amounts of HCl. Thus, the trend in hydrogen evolution rate might be attributable to the need for a balance between the light penetration depth and charge carrier diffusion length.

To further elucidate the effect of ZIS shell thickness with regard to crystallinity, hydrogen evolution rates of three samples synthesized from the selected concentrations of ZIS precursor with various amounts of HCl, SiO_2@3×ZIS E-2, SiO_2@2×ZIS E-3, and SiO_2@ZIS E-4, bearing nearly similar ZIS shell thicknesses (see Table S2) were compared (Figure 8). Among the samples with similar shell thicknesses, those

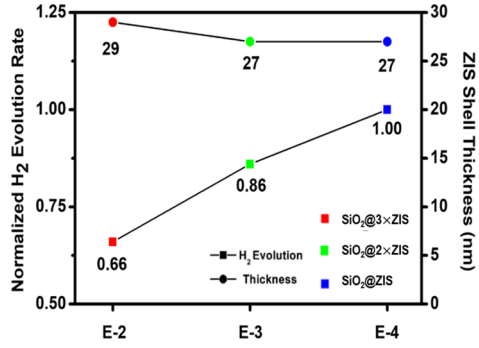

Figure 8. Photocatalytic hydrogen evolution rate of SiO_2@ZIS (E-2, E-3, and E-4) synthesized with varying concentrations of ZIS precursor and varied amounts of HCl in ethanol, bearing similar ZIS shell thickness.

synthesized with larger amounts of HCl, exhibiting enhanced crystallinity, demonstrated higher rates of hydrogen evolution. It is noteworthy that although the shell thicknesses measured by calculating the difference in the diameters of bare and ZIS-coated SiO_2 are not precise, the shell thickness can be controlled by varying the amounts of HCl added and the concentration of precursors. Further, discerning the trend of the effect of ZIS shell thickness along with crystallinity on the hydrogen evolution rate of SiO_2@ZIS core−shell nanoparticles was also possible. Furthermore, the hydrogen evolution rate achieved in this work was similar to or better than that of most of the previously reported ZIS particles (Table S3). It is worth mentioning that hydrogen evolution rate is also highly

https://dx.doi.org/10.1021/acsami.0c20716
ACS Appl. Mater. Interfaces 2021, 13, 4043−4050

dependent on measurement conditions and methods which can vary. Finally, Figure 9 shows the photostability and

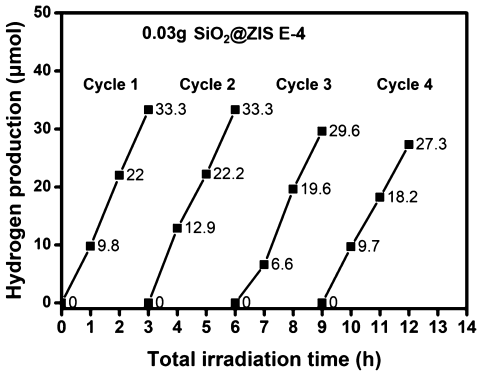

Figure 9. Photo-stability and re-usability of SiO_2@ZIS E-4 core−shell nanoparticles tested for four cycles of hydrogen evolution.

reusability of the synthesized shell-size-tunable SiO_2@ZIS core−shell nanoparticles. After four cycles of repeated photocatalytic hydrogen evolution tests, the sample SiO_2 @ ZIS E-4 showed only a slight decrease in the rate of hydrogen evolution.

CONCLUSIONS

The surface modification on SiO_2 core nanoparticles with MPS promoted the nucleation of ZIS, leading to uniform coverage. The crystallinity and coverage of ZIS in the SiO_2@ZIS core−shell nanoparticles were improved by using microwave-assisted hydrothermal synthesis in ethanol with the addition of HCl. The hydrogen evolution rate was enhanced as well. The shell thickness of ZIS could be easily tuned by adding selected concentrations of ZIS precursor without negatively affecting the ZIS crystallinity or the rate of hydrogen production. This facile procedure paves the way to generate a more complex structure, GS-NS@dielectric@photocatalyst, for the optimization of solar hydrogen production.

ASSOCIATED CONTENT

Supporting Information

The Supporting Information is available free of charge at https://pubs.acs.org/doi/10.1021/acsami.0c20716.

Schematic of the hydrogen generation setup; size distribution of modified SiO_2; ZIS shell thickness with varying concentrations of the precursor and amount of HCl along with normalized hydrogen evolution rate for samples synthesized with 100 μL HCl; TEM image of SiO_2 core nanoparticles; size distribution histogram of SiO_2 core nanoparticles; TEM images of SiO_2 and MPS-modified SiO_2 core nanoparticles; XPS spectra of SiO_2 and MPS-modified SiO_2 core nanoparticles; TEM images of ZIS on bare SiO_2 and ZIS on MPS-modified SiO_2 synthesized in water; SiO_2@ZIS synthesized in ethanol with 150 μL of HCl; TEM images of SiO_2@ZIS core−shell nanoparticles with different concentrations of precursor in ethanol and amounts of HCl; and hydrogen evolution rate and ZIS shell thickness of SiO_2@ZIS, SiO_2@2×ZIS, and SiO_2@3×ZIS synthesized with 20 μL (E-2), 50 μL (E-3), and 100 μL (E-4) of HCl (PDF)

AUTHOR INFORMATION

Corresponding Author

Tai-Chou Lee − *Department of Chemical and Materials Engineering, National Central University, Jhongli City 32001, Taiwan;* orcid.org/0000-0002-1695-1201; Email: taichoulee@ncu.edu.tw

Authors

Mrinalini Mishra − *Department of Chemical and Materials Engineering, National Central University, Jhongli City 32001, Taiwan; Sustainability Science and Engineering Program, International College, Tunghai University, Taichung 40704, Taiwan;* orcid.org/0000-0002-5945-2170

Yen-Chen Huang − *Department of Chemical and Materials Engineering, National Central University, Jhongli City 32001, Taiwan*

Peng-Hua Wang − *Department of Chemical and Materials Engineering, National Central University, Jhongli City 32001, Taiwan*

Si-Ping Liu − *Department of Chemical and Materials Engineering, National Central University, Jhongli City 32001, Taiwan*

T. Randall Lee − *Department of Chemistry, University of Houston, Houston, Texas 77204-5003, United States;* orcid.org/0000-0001-9584-8861

Complete contact information is available at: https://pubs.acs.org/10.1021/acsami.0c20716

Author Contributions

‖M.M. and Y.-C.H. made equal contributions to this work.

Notes

The authors declare no competing financial interest.

ACKNOWLEDGMENTS

Research at the National Central University was supported by the Ministry of Science and Technology of Taiwan (MOST 108-2221-E-008-04-MY3; MOST 104-2628-E-008-003-MY3) and the US Air Force Office of Scientific Research (FA2386-17-1-4028). Research at the University of Houston was supported by the US Air Force Office of Scientific Research (FA9550-20-1-0349; 20RT0302) and the Robert A. Welch Foundation (E-1320).

REFERENCES

(1) Grätzel, M. Photoelectrochemical Cells. *Nature* **2001**, *414*, 338−344.

(2) Takata, T.; Pan, C.; Nakabayashi, M.; Shibata, N.; Domen, K. Fabrication of a Core−Shell-Type Photocatalyst via Photodeposition of Group IV and V Transition Metal Oxyhydroxides: An Effective Surface Modification Method for Overall Water Splitting. *J. Am. Chem. Soc.* **2015**, *137*, 9627−9634.

(3) Maeda, K.; Domen, K. Photocatalytic Water Splitting: Recent Progress and Future Challenges. *J. Phys. Chem. Lett.* **2010**, *1*, 2655−2661.

(4) Kudo, A. Photocatalyst Materials for Water Splitting. *Catal. Surv. Asia* **2003**, *7*, 31−38.

(5) Shiga, Y.; Umezawa, N.; Srinivasan, N.; Koyasu, S.; Sakai, E.; Miyauchi, M. A Metal Sulfide Photocatalyst Composed of Ubiquitous Elements for Solar Hydrogen Production. *Chem. Commun.* **2016**, *52*, 7470−7473.

(6) Tsuji, I.; Kato, H.; Kudo, A. Visible-Light-Induced H_2 Evolution from an Aqueous Solution Containing Sulfide and Sulfite over a ZnS−$CuInS_2$−$AgInS_2$ Solid-Solution Photocatalyst. *Angew. Chem., Int. Ed.* **2005**, *44*, 3565−3568.

https://dx.doi.org/10.1021/acsami.0c20716
ACS Appl. Mater. Interfaces 2021, 13, 4043−4050

(7) Septina, W.; Gunawan; Ikeda, S.; Harada, T.; Higashi, M.; Abe, R.; Matsumura, M. Photosplitting of Water from Wide-Gap $Cu(In,Ga)S_2$ Thin Films Modified with a CdS Layer and Pt Nanoparticles for a High-Onset-Potential Photocathode. *J. Phys. Chem. C* **2015**, *119*, 8576−8583.
(8) Zhu, Y.-J.; Chen, F. Microwave-Assisted Preparation of Inorganic Nanostructures in Liquid Phase. *Chem. Rev.* **2014**, *114*, 6462−6555.
(9) Shen, S.; Chen, J.; Wang, X.; Zhao, L.; Guo, L. Microwave-Assisted Hydrothermal Synthesis of Transition-Metal Doped $ZnIn_2S_4$ and Its Photocatalytic Activity for Hydrogen Evolution under Visible Light. *J. Power Sources* **2011**, *196*, 10112−10119.
(10) Hu, X.; Yu, J. C.; Gong, J.; Li, Q. Rapid Mass Production of Hierarchically Porous $ZnIn_2S_4$ Submicrospheres via a Microwave-Solvothermal Process. *Cryst. Growth Des.* **2007**, *7*, 2444−2448.
(11) Tang, X.; Tay, Q.; Chen, Z.; Chen, Y.; Goh, G. K. L.; Xue, J. Cu−In−Zn−S Nanoporous Spheres for Highly Efficient Visible-Light-Driven Photocatalytic Hydrogen Evolution. *New J. Chem.* **2013**, *37*, 1878−1882.
(12) Shen, S.; Zhao, L.; Zhou, Z.; Guo, L. Enhanced Photocatalytic Hydrogen Evolution over Cu-Doped $ZnIn_2S_4$ under Visible Light Irradiation. *J. Phys. Chem. C* **2008**, *112*, 16148−16155.
(13) Hou, J.; Yang, C.; Cheng, H.; Wang, Z.; Jiao, S.; Zhu, H. Ternary 3D Architectures of CdS QDs/Graphene/$ZnIn_2S_4$ Heterostructures for Efficient Photocatalytic H_2 Production. *Phys. Chem. Chem. Phys.* **2013**, *15*, 15660−15668.
(14) Xu, B.; He, P.; Liu, H.; Wang, P.; Zhou, G.; Wang, X. A 1D/2D Helical CdS/$ZnIn_2S_4$ Nano-Heterostructure. *Angew. Chem., Int. Ed.* **2014**, *53*, 2339−2343.
(15) Li, Y.; Wang, J.; Peng, S.; Lu, G.; Li, S. Photocatalytic Hydrogen Generation in the Presence of Glucose over ZnS-Coated $ZnIn_2S_4$ under Visible Light Irradiation. *Int. J. Hydrogen Energy* **2010**, *35*, 7116−7126.
(16) Chai, B.; Peng, T.; Zeng, P.; Zhang, X. Preparation of a MWCNTs/$ZnIn_2S_4$ Composite and Its Enhanced Photocatalytic Hydrogen Production under Visible-Light Irradiation. *Dalton Trans.* **2012**, *41*, 1179−1186.
(17) Li, C.-H.; Li, M.-C.; Liu, S.-P.; Jamison, A. C.; Lee, D.; Lee, T. R.; Lee, T.-C. Plasmonically Enhanced Photocatalytic Hydrogen Production from Water: The Critical Role of Tunable Surface Plasmon Resonance from Gold−Silver Nanoshells. *ACS Appl. Mater. Interfaces* **2016**, *8*, 9152−9161.
(18) Chen, Y.; Tian, G.; Ren, Z.; Pan, K.; Shi, Y.; Wang, J.; Fu, H. Hierarchical Core−Shell Carbon Nanofiber@$ZnIn_2S_4$ Composites for Enhanced Hydrogen Evolution Performance. *ACS Appl. Mater. Interfaces* **2014**, *6*, 13841−13849.
(19) Gou, X.; Cheng, F.; Shi, Y.; Zhang, L.; Peng, S.; Chen, J.; Shen, P. Shape-Controlled Synthesis of Ternary Chalcogenide $ZnIn_2S_4$ and $CuIn(S,Se)_2$ Nano-/Microstructures via Facile Solution Route. *J. Am. Chem. Soc.* **2006**, *128*, 7222−7229.
(20) Shen, S.; Zhao, L.; Guo, L. Crystallite, Optical and Photocatalytic Properties of Visible-Light-Driven $ZnIn_2S_4$ Photocatalysts Synthesized via a Surfactant-Assisted Hydrothermal Method. *Mater. Res. Bull.* **2009**, *44*, 100−105.
(21) Shen, S.; Zhao, L.; Guo, L. Cetyltrimethylammoniumbromide (CTAB)-Assisted Hydrothermal Synthesis of $ZnIn_2S_4$ as an Efficient Visible-Light-Driven Photocatalyst for Hydrogen Production. *Int. J. Hydrogen Energy* **2008**, *33*, 4501−4510.
(22) Choi, W.; Choi, J. Y.; Song, H. Regulation of Electron-Hole Recombination Kinetics on Uniform Metal-Semiconductor Nanostructures for Photocatalytic Hydrogen Evolution. *APL Mater.* **2019**, *7*, 100702.
(23) Wang, Q.; Domen, K. Particulate Photocatalysts for Light-Driven Water Splitting: Mechanisms, Challenges, and Design Strategies. *Chem. Rev.* **2020**, *120*, 919−985.
(24) Chen, J.; Dong, C.-L.; Du, Y.; Zhao, D.; Shen, S. Nanogap Engineered Plasmon-Enhancement in Photocatalytic Solar Hydrogen Conversion. *Adv. Mater. Interfaces* **2015**, *2*, 1500280.
(25) Vongsavat, V.; Vittur, B. M.; Bryan, W. W.; Kim, J.-H.; Lee, T. R. Ultrasmall Hollow Gold-Silver Nanoshells with Extinctions Strongly Red-Shifted to the near-Infrared. *ACS Appl. Mater. Interfaces* **2011**, *3*, 3616−3624.
(26) Cushing, S. K.; Li, J.; Meng, F.; Senty, T. R.; Suri, S.; Zhi, M.; Li, M.; Bristow, A. D.; Wu, N. Photocatalytic Activity Enhanced by Plasmonic Resonant Energy Transfer from Metal to Semiconductor. *J. Am. Chem. Soc.* **2012**, *134*, 15033−15041.
(27) Shen, S.; Zhao, L.; Guo, L. Morphology, Structure and Photocatalytic Performance of $ZnIn_2S_4$ Synthesized via a Solvothermal/Hydrothermal Route in Different Solvents. *J. Phys. Chem. Solids* **2008**, *69*, 2426−2432.
(28) Chai, B.; Peng, T.; Zeng, P.; Zhang, X.; Liu, X. Template-Free Hydrothermal Synthesis of $ZnIn_2S_4$ Floriated Microsphere as an Efficient Photocatalyst for H_2 Production under Visible-Light Irradiation. *J. Phys. Chem. C* **2011**, *115*, 6149−6155.
(29) Li, F.; Luo, J.; Chen, G.; Fan, Y.; Huang, Q.; Luo, Y.; Li, D.; Meng, Q. Hydrothermal Synthesis of Zinc Indium Sulfide Microspheres with Ag^+ Doping for Enhanced H_2 Production by Photocatalytic Water Splitting under Visible Light. *Catal. Sci. Technol.* **2014**, *4*, 1144−1150.
(30) Chen, Z.; Li, D.; Zhang, W.; Chen, C.; Li, W.; Sun, M.; He, Y.; Fu, X. Low-Temperature and Template-Free Synthesis of $ZnIn_2S_4$ Microspheres. *Inorg. Chem.* **2008**, *47*, 9766−9772.
(31) Stöber, W.; Fink, A.; Bohn, E. Controlled Growth of Monodisperse Silica Spheres in the Micron Size Range. *J. Colloid Interface Sci.* **1968**, *26*, 62−69.
(32) Kim, J.-H.; Chung, H.-W.; Lee, T. R. Preparation and Characterization of Palladium Shells with Gold and Silica Cores. *Chem. Mater.* **2006**, *18*, 4115−4120.
(33) Lu, Z.; Gao, C.; Zhang, Q.; Chi, M.; Howe, J. Y.; Yin, Y. Direct Assembly of Hydrophobic Nanoparticles to Multifunctional Structures. *Nano Lett.* **2011**, *11*, 3404−3412.
(34) Zheng, F.; Zhang, N.; Hu, B. Mn(II) Imprinted 3-Mercaptopropyltrimethoxysilane (MPTS)-Silica Coated Capillary Microextraction on-Line Hyphenated with Inductively Coupled Plasma Mass Spectrometry for the Determination of Trace Mn(II) in Biological Samples. *J. Anal. At. Spectrom.* **2011**, *26*, 1521−1525.
(35) Song, J.; Kim, H.; Jang, Y.; Jang, J. Enhanced Antibacterial Activity of Silver/Polyrhodanine-Composite-Decorated Silica Nanoparticles. *ACS Appl. Mater. Interfaces* **2013**, *5*, 11563−11568.
(36) Sapsford, K. E.; Algar, W. R.; Berti, L.; Gemmill, K. B.; Casey, B. J.; Oh, E.; Stewart, M. H.; Medintz, I. L. Functionalizing Nanoparticles with Biological Molecules: Developing Chemistries That Facilitate Nanotechnology. *Chem. Rev.* **2013**, *113*, 1904−2074.
(37) Wu, J.; Ling, L.; Xie, J.; Ma, G.; Wang, B. Surface Modification of Nanosilica with 3-Mercaptopropyl Trimethoxysilane: Experimental and Theoretical Study on the Surface Interaction. *Chem. Phys. Lett.* **2014**, *591*, 227−232.
(38) Kandjani, A. E.; Sabri, Y. M.; Periasamy, S. R.; Zohora, N.; Amin, M. H.; Nafady, A.; Bhargava, S. K. Controlling Core/Shell Formation of Nanocubic p-Cu_2O/n-ZnO Toward Enhanced Photocatalytic Performance. *Langmuir* **2015**, *31*, 10922−10930.
(39) Joo, J. B.; Zhang, Q.; Dahl, M.; Lee, I.; Goebl, J.; Zaera, F.; Yin, Y. Control of the Nanoscale Crystallinity in Mesoporous TiO_2 Shells for Enhanced Photocatalytic Activity. *Energy Environ. Sci.* **2012**, *5*, 6321−6327.
(40) Lin, L.-H.; Wu, C.-C.; Lee, T.-C. Growth of Crystalline $AgIn_5S_8$ Thin Films on Glass Substrates from Aqueous Solutions. *Cryst. Growth Des.* **2007**, *7*, 2725−2732.
(41) Castro, E. A. Kinetics and Mechanisms of Reactions of Thiol, Thiono, and Dithio Analogues of Carboxylic Esters with Nucleophiles. *Chem. Rev.* **1999**, *99*, 3505−3524.
(42) Gosavi, R. K.; Rao, C. N. R. Infrared Absorption Spectra of Metal Complexes of Alkylthioureas and Some Related Ligands. *J. Inorg. Nucl. Chem.* **1967**, *29*, 1937−1945.

https://dx.doi.org/10.1021/acsami.0c20716
ACS Appl. Mater. Interfaces 2021, 13, 4043−4050